Evaluation of Single-Ended Impedance-Based Transmission Fault Location Using Fixed and Variable Window Phasor Estimation Approaches

R. L. A. Reis, F. V. Lopes, E. J. S. Leite Jr., G. Zat, J. V. Souza, A. Scheid, T. G. Jahn

***Abstract*—In this paper, the performances of fixed and variable window size phasor-based techniques reported in the literature are evaluated on a classical one-terminal impedance-based fault locator, pointing out the challenges and alternatives for applications in transmission systems equipped with high-speed protection functions. To do so, several Alternative Transients Program (ATP) fault simulations were carried out in a 230 kV/60 Hz power network, varying their parameters such as type, location, inception angle and resistance. The obtained results attest that phasors estimated from variable window size strategies may improve the fault locator performance, even in the first cycles after the disturbance occurrence, appearing themselves as potential alternatives to be applied in combination with high-speed phasor-based protection routines.**

***Keywords*—Fault location, high-speed protection, phasor-based techniques, transmission systems.**

I. Introduction

In the case of transmission line (TL) short-circuit occurrences, power utilities need to properly identify the fault points as quickly as possible, in order to speed up the system restoration process and its supply. In this way, to reduce the outage times, researches and commercially-available protective relays move toward the development of more robust and faster protection and fault location functions, such as in the cases of time-domain technologies, for example [1].

Although traveling wave-based fault location techniques are reported as one of the most robust functionalities, spreading out their use over the years, they commonly work combined with auxiliary phasor-based solutions, especially for single-ended purposes [2]. Besides, phasor-based fault location methods are still predominant in the most numerical protective relays installed in the field. In this context, irrespective of the used protection scheme, the short-circuit distance is estimated from the voltage and current phasors computed at the available fault period data window [3]. Typically, this fault period ranges from 3 to 5 fundamental cycles, by considering the performance of both conventional phasor-based protection functions (with fixed data window length) and the corresponding electromechanical circuit breaker (CB) opening time [1].

On the other hand, by using high-speed protective relays, the trip signals are sent in just a few milliseconds [4]. In such cases, although benefits to the power transmission grid are noticed, such as improving the stability margin and reducing the equipment damages, challenges to phasor-based fault location algorithms may arise due to the fault period reduction. In fact, the computed phasors may not be able to converge in a shorter fault period, which may affect the performance of such routines, highlighting the need for alternatives that may provide more accurate phasor estimations in a shorter period.

Traditionally, most of the phasor estimation techniques use fixed data window lengths (FW) to compute the corresponding fundamental components, which are usually based on the Fourier Transform [5], [6]. In such cases, more accurate fault location estimations are obtained when voltage and current phasor samples are taken as input data in at least three cycles after the fault inception [7], which is a reasonable time for offline applications and conventional protection performance times. For a smaller number of cycles, the phasors may not reach their convergence stage due to the impacts of DC components and presence of pre-fault samples in the data window, which may affect the accuracy of the phasor-based fault location routines. However, for systems equipped with high-speed protective functions, the disturbances may be extinguished after such a period of time, and the fault location techniques' reliability may be compromised.

To provide solutions for speeding up the computed phasors convergences, phasor estimation techniques with a variable size data window are reported in the literature. In [8], for example, a method able to operate with any number of data window lengths is proposed, in which such length can be varied by an auxiliary routine, as reported in [9]. In [10], in turn, a phasor-based with variable size window (VW) algorithm is proposed, which is designed as a bandpass filter.

Analyses comparing the performance of FW and VW phasor-based routines on distance protection functions are carried out in [9], in which more accurate apparent impedance estimations are obtained in a shorter period in relation to the FW technique. Similar analyses are performed in [11], in which faster trip commands were obtained for the first zone protection function. In this scenario, despite FW and VW phasor-based methods are reported in the literature for protection applications, comparative analysis regarding their performances for fault location purposes are scarcely reported,

This work was sponsored by Itaipu Technological Park Foundation (FPTI-BR).

R. L. A. Reis and F. V. Lopes are with Federal University of Paraíba (UFPB), Brazil (email: raphael.leite, felipelopes@cear.ufpb.br). E. J. S. Leite Jr. is an independent author (email: eduardoleitejr@gmail.com). G. Zat, J. V. Souza and T. G. Jahn are with Itaipu Technological Park Foundation (FPTI-BR), Brazil (email: guilherme.zat, jonas.souza, tales.jahn@pti.org.br). A. Scheid is an independent author (email: avs.009@gmail.com).

Paper submitted to the International Conference on Power Systems Transients (IPST2023) in Thessaloniki, Greece, June 12-15, 2023.

even for cases in which high-speed protection functions can reduce the available fault period to be used as input data to the corresponding fault locators.

Hence, thorough comparative analyses regarding FW and VW phasor-based routines reported in the literature are addressed in this paper, pointing out the reliability of using the first cycles after the short-circuit inception to estimate the disturbance point, taking into account the performance of high-speed protection functions. To do so, several Alternative Transients Program (ATP) fault simulations are carried out in a 230 kV/60 Hz power network, varying the fault parameters, such as type, location, inception angle and resistance. In each case, fault distances are estimated as a function of the number of cycles taken as input data to a classical single-ended impedance-based fault location method.

II. Fundamental Principles

A. Fixed Window Phasor-Based Technique (FW)

Here, the classical Full Cycle Discrete Fourier Transform (FCDFT) is considered [5], which computes the real (Y_{real}) and imaginary (Y_{im}) components of a discrete signal $y(m)$ within a fixed data window length of N samples per cycle, as:

$$Y_{real}(k) = \frac{2}{N}\sum_{m=0}^{N-1} y(k-N+m)\cdot\cos\left(\frac{2\pi}{N}m\right), \quad (1a)$$

$$Y_{im}(k) = -\frac{2}{N}\sum_{m=0}^{N-1} y(k-N+m)\cdot\sin\left(\frac{2\pi}{N}m\right), \quad (1b)$$

being $y(k-N+m)$ the m-th sample of the k-th data window of the digital signal y.

The mimic filter reported in [12] is combined with the FCDFT algorithm to minimize the impacts of DC components on the estimated phasors, resulting in the FW method used in the following analysis. Basically, it consists in a high-pass digital filter with a delay computed from the system L/R ratio, according to:

$$y(k)^* = K\left[(1+\tau_d)\,y(k) - \tau_d y(k-1)\right] , \quad (2)$$

in which $y(k)^*$ is the filtered signal at the sample k, $y(k)$ and $y(k-1)$ are the original signal y at samples k and $k-1$, respectively, τ_d is the designed time constant of the mimic filter (in sample value), and K is the filter gain, which is computed to have unit gain at the fundamental frequency, being computed as follows:

$$K = \sqrt{\frac{1}{\left[(1+\tau_d) - \tau_d\cos\left(\frac{2\pi}{N}\right)\right]^2 + \left[\tau_d\sin\left(\frac{2\pi}{N}\right)\right]^2}} , \quad (3)$$

B. Variable Window Phasor-Based Technique (VW)

VW phasor estimation routines may resize the used data window right after the disturbance detection. Such procedures aim to reduce the transient period in which pre- and post-fault samples are included in the analyzed data window to compute the associated phasors. Basically, the strategy reported in [10] uses a variable size window of length M to estimate the corresponding voltage and current phasors, assuming a fraction of N after the short-circuit inception, progressively increasing itself up to $M = N$, which corresponds to the time instant when the "steady-state" fault period is reached.

The discrete signal y is filtered by means of orthogonal filters, whose the cosine- and sine-shaped windows for the direct h_D and quadrature h_Q filters are [10]:

$$h_D(k) = \cos\left[\frac{2\pi(k-0.5)}{N}\right], \quad (4a)$$

$$h_Q(k) = \sin\left[\frac{2\pi(k-0.5)}{N}\right], \quad (4b)$$

for $k = 1,..,N/2$. The N window length is computed as:

$$N = 2\left[\text{floor}\left(\frac{0.5 f_S}{f_{nom}}\right) + 1\right] , \quad (5)$$

in which f_S and f_{nom} are the sampling rate and the network nominal frequency, respectively. The orthogonal components of the signal y are then computed as:

$$y_D(n) = \sum_{k=1}^{k=M/2} h_D(k)\cdot\rho, \quad (6a)$$

$$y_Q(n) = \sum_{k=1}^{k=M/2} h_Q(k)\cdot\rho, \quad (6b)$$

being ρ equal to:

$$\rho = y(n-M/2-k+1) + y(n-M/2+k) . \quad (7)$$

The gain of the process described in (6) for the fundamental frequency component is dependent on the length of M [13]. To compensate it, the components y_D and y_Q are multiplied by the gain-correcting coefficients C_D and C_Q, respectively, which are:

$$C_D = \left[\frac{M}{2}\cdot\left(\frac{\sin(A)}{A} + \frac{\sin(B)}{B}\right)\right]^{-1}, \quad (8a)$$

$$C_Q = \left[\frac{M}{2}\cdot\left(\frac{\sin(A)}{A} - \frac{\sin(B)}{B}\right)\right]^{-1}, \quad (8b)$$

being:

$$A = \pi\cdot\frac{M}{N}\cdot\left(\frac{f}{f_{nom}} - 1\right), \quad (9a)$$

$$B = \pi\cdot\frac{M}{N}\cdot\left(\frac{f}{f_{nom}} + 1\right). \quad (9b)$$

As a result, in the considered VW technique, the phasor components of the signal y, named as y_C, can be expressed according to:

$$y_C = y_D\cdot C_D + j y_Q\cdot C_Q . \quad (10)$$

It is worth mentioning that, for the subsequent analysis, the FW and VW routines were implemented accordingly to references [5] and [10], respectively. For the FW technique, a mimic filter was also considered to minimize the decaying DC components, as classically suggested in the literature [12], [14]. On the other hand, since mimic filters are not taken into account in [10], they were not considered in the implemented VW method.

To illustrate the performance of the FW and VW phasor estimation techniques, an AG fault was applied at 20 km away from the local bus of the power system described in section III. Considering a fault inception angle of 90°, the voltage signal v_a and its phasors computed by the FW ($|\hat{V}_a|$ FW) and VW ($|\hat{V}_a|$ VW) algorithms are presented in Fig. 1(a). The corresponding current waveform i_a and the phasors $|\hat{I}_a|$ FW and $|\hat{I}_a|$ VW are shown in Fig. 1(b). The same electrical signals are depicted in Fig. 2 for a 0° fault inception angle. To allow comparative analysis, voltage and current phasors are also estimated by the FW routine, but without the considered mimic filter, being represented in Figs. 1 and 2 by $|\hat{V}_a|$ FW$_{nm}$ and $|\hat{I}_a|$ FW$_{nm}$, respectively. The sampling frequency for both FW and VW techniques is taken as 34 samples/cycle, as suggested in [10] for the VW method application.

As shown in Figs. 1 and 2, the phasors estimated by the VW routine tend to reach their convergence faster than the ones computed by the FW algorithm, especially for cases without significant decaying DC components (inception angles different from 0°), since the implemented VW technique does not take into account mimic filters. Such performance is similar to the FW routine with no mimic filter (phasors $|\hat{V}_a|$ FW$_{nm}$ and $|\hat{I}_a|$ FW$_{nm}$). In fact, right after the short-circuit occurrence, the data window length is resized to contain only fault data information, in such a way that the transient period in which both pre- and post-fault samples are taken into account in the analyzed window is considerably reduced. As a consequence, the estimated phasors quickly go toward a narrow range of their final value. However, since a fixed window length is considered by the FW technique, such transient period with both pre- and post-fault samples is bigger, leading the estimated phasors to converge slower as the windows move along the electrical signal samples.

For these cases, the CBs open their terminals with approximately 3 cycles, whose instant corresponds to the time in which more accurate FW phasors are estimated. As a consequence, for fault scenarios in which the time of the protection operation and the CBs opening time are smaller than this value, the computed phasors may not fully stabilize, leading such information to be transferred to the fault location routines. Differently, the VW phasors have reached more reliable results sooner in the evaluated situations.

C. Single-Ended Impedance-Based Fault Location

Single-ended phasor-based fault location methods are typically embedded on most of the protective devices in operation worldwide [1]. Fundamentally, they compute the apparent impedance between the monitored TL bus and the short-circuit point to estimate the fault distance. In this paper, the classical method reported in [15] was implemented, whose fault distance d is given by:

$$d = \frac{\text{im}(\hat{V}_L \cdot \Delta\hat{I}_L^*)}{\text{im}(Z_{L1} \cdot \hat{I}_L \cdot \Delta\hat{I}_L^*)} \ , \tag{11}$$

being "im" the imaginary part, $\hat{V}_\text{L}$ the estimated voltage phasor, $\hat{I}_\text{L}$ the computed current phasor, and $\Delta\hat{I}_\text{L}$ the "pure fault" current phasor measured at the monitored TL end. The values of $\hat{V}_\text{L}$, $\hat{I}_\text{L}$ and $\Delta\hat{I}_\text{L}$ depend on the fault type [1].

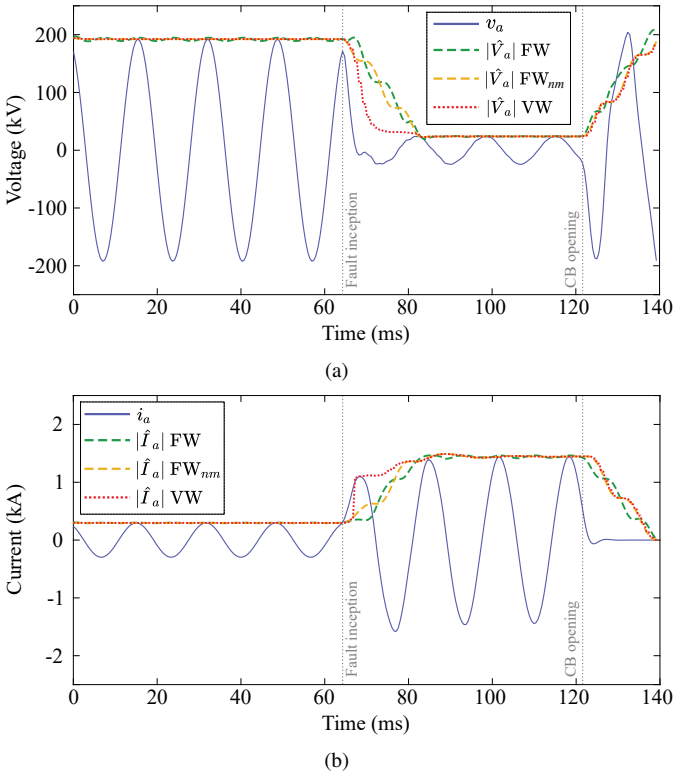

Fig. 1. Estimated phasors from FW and VW methods for an AG fault with 90° inception angle: (a) voltages; (b) currents.

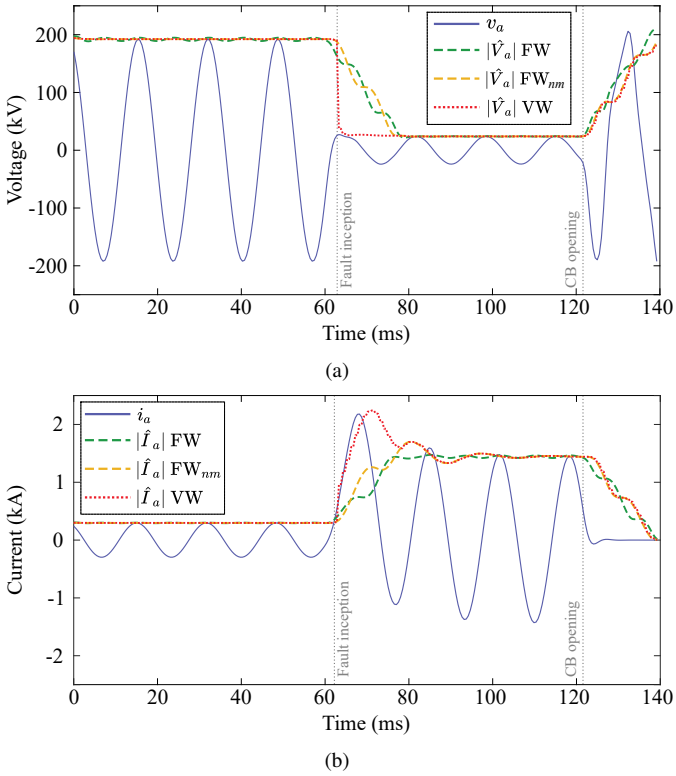

Fig. 2. Estimated phasors from FW and VW methods for an AG fault with 0° inception angle: (a) voltages; (b) currents.

III. Analysis and Results

To evaluate the performance of the FW and VW phasor estimation routines on the considered impedance-based fault location method, ATP short-circuit simulations were carried out at d km away from the Local bus of the power grid shown in Fig. 3, with a time step of 10 μs. The line length ℓ was taken as 100 km. The power system topology is described in [16] and its parameters were adjusted from real Brazilian transmission networks.

It is well-known the dynamic behavior induced by coupling capacitor voltage transformers (CCVTs) during faults, as well as the impacts of current transformers (CTs) saturation on phasor-based routines [7]. However, the researches and practical developments are moving toward the development of compensation techniques to provide high-fidelity voltage measurements in a wider frequency spectrum, such as the use of optical voltage transformers [17], the reconstruction of voltage signals based on numerical integration of current measurements through the CCVT capacitive stacks [18], or even by means of techniques based on recursive digital filters [19].

Regarding the CTs, they typically present a flat frequency response over a wide bandwidth, being not a cause for concern for the most demanding applications when they are unsaturated [7]. Tests were previously carried out in the evaluated power grid shown in Fig. 3, considering even cases for faults near the CT terminals, but they have not led the equipment to saturate. Thus, the saturation effects were not taken into account during the performed analyses.

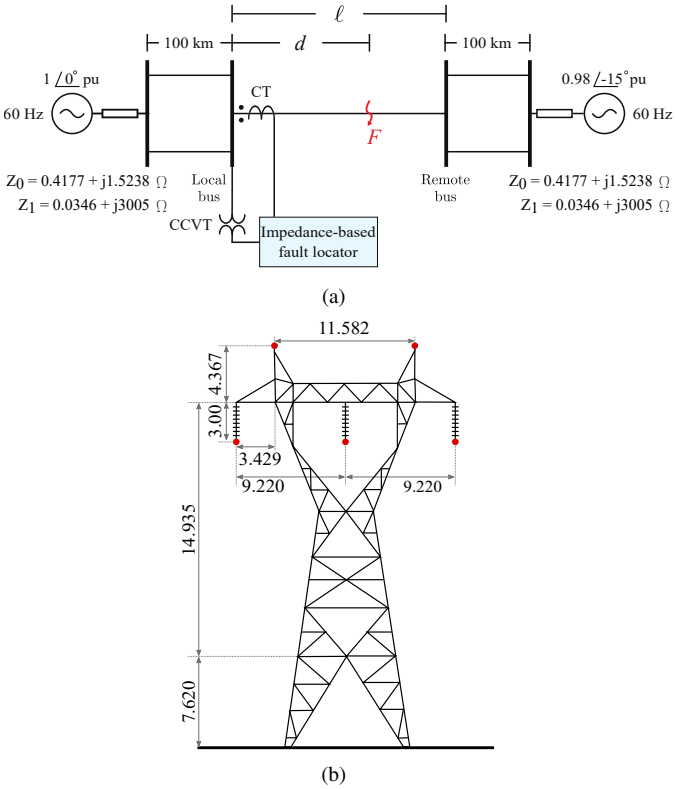

Fig. 3. 230 kV/60 Hz power network used in the fault simulations: (a) Single-line diagram; (b) tower structure with distances in meters.

In this way, since the main goal here is evaluating the performance of both FW and VW functionalities for cases with high-speed protections, it is assumed that the voltage and current signals are measured with acceptable accuracy in the following analyses. Tests with a classical CCVT digital model reported in [20] for protection studies are presented in section IV-B. Besides, as the focus of the following evaluations are on fault-locating purposes, distinguishing between short-circuits and other transient events is out of the scope of this work.

Basically, 504 ATP short-circuit simulations were carried out, varying the fault parameters, such as resistance, type, location, and inception angle. The fault simulation variables are presented in Table I. To consider the performance of high-speed protection functions, the CBs should be opened before three power cycles. However, to allow comparative analysis during the instants in which phasor-based algorithms estimate more convergent fundamental components, the CBs were opened right after three cycles.

It is worth mentioning that the faults were represented using traditional linear models, as the ones reported in [1], i.e., the effects of primary electric arcs were not considered in the simulations. In addition, although the electric arc induced during CBs tripping operation may affect the total fault time, the analyses carried out in this paper are focused on evaluating the samples during only the fault period, in such a way that samples right after the CB opening are not taken into account. Thus, electric arc modeling due to the CB operation was not implemented in the evaluated short-circuit scenarios.

The ATP records are used as input data for each evaluated phasor-based method, resulting in the distances estimations d_{FW} and d_{VW} for both FW and VW routines, respectively. To investigate the impact of choosing different voltage and current phasors as a function of the number of cycles after the fault detection, the fault distances were computed taken 1, 2 and 3 cycles after the disturbance occurrence as input data to the evaluated impedance-based algorithm. In such cases, $d_{FW,1}$ and $d_{VW,1}$ mean the fault distances estimated by FW and VW functions, respectively, considering samples taken from 1 cycle after the fault detection, $d_{FW,2}$ and $d_{VW,2}$ for 2 cycles and $d_{FW,3}$ and $d_{VW,3}$ for 3 cycles. In each fault simulation, the absolute percentage error is computed as $\varepsilon = (|d-\tilde{d}|/\ell)\cdot 100\%$, being $\tilde{d}$ the estimated fault point d_{FW} or d_{VW}.

The obtained results are shown in Figs. 4, 5 and 6 as scatter plots, in which the estimated errors assuming phasors from the VW technique are presented at the y-axis, whereas the obtained errors from the FW phasor-based routine are shown at the x-axis.

TABLE I
Fault variables used in the ATP simulations

Simulation variables	Values
Fault location (km)	10, 20, 30, 40, 50, 60, 70, 80, 90
Fault type	AG, BC, BCG, ABC
Inception angle (°)	1, 30, 60, 90, 120, 150
Fault resistance (Ω)	1, 10

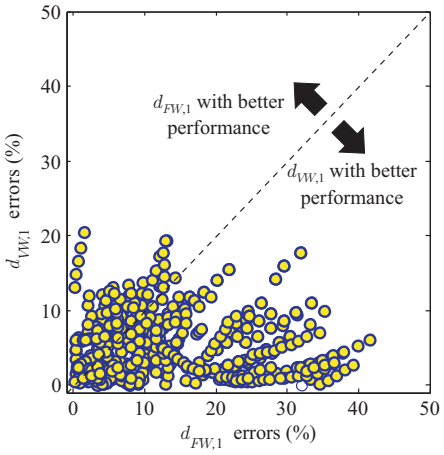

Fig. 4. Scatter plot of the estimated fault location errors from both FW and VW phasor-based methods considering 1 cycle as input data.

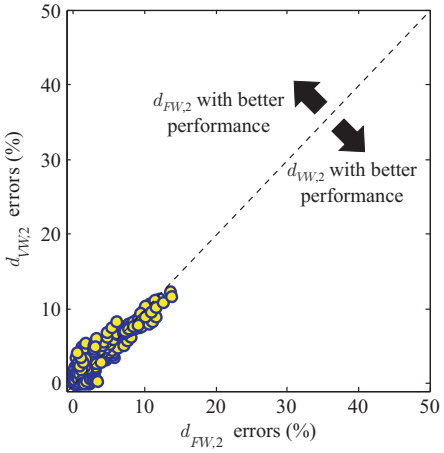

Fig. 5. Scatter plot of the estimated fault location errors from both FW and VW phasor-based methods considering 2 cycles as input data.

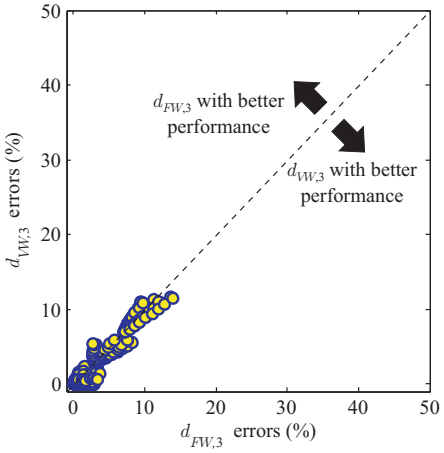

Fig. 6. Scatter plot of the estimated fault location errors from both FW and VW phasor-based methods considering 3 cycles as input data.

From the obtained results presented in Figs. 5 and 6, the estimated fault location errors assuming 2 and 3 cycles from both FW and VW routines as input data presented similar responses, in such a way that in this period of time, the voltage and current fundamental components tend to converge around the final value of their corresponding phasors, since the fault-induced transients are almost completely damped in such period. As a consequence, as the data window moves along samples at the fault period, the performance of both FW and VW are similar, once the resized window length for the VW technique is already incremented until reaches the same number of samples as used in FW methods.

On the other hand, if the cases of CBs opening their terminals before 3 power cycles, the data information about the fault period would be reduced. In such cases, the best estimations were provided by the VW algorithm, as depicted in Fig. 4, since most of the errors of $d_{FW,1}$ are higher than the ones of $d_{VW,1}$ (higher quantity of cases below the graphic diagonal line). In this situation, the VW estimated phasors tend to reach their convergent values shorter than the ones provided by the FW algorithms, resulting in better estimations when just voltage and current samples are taken from 1 cycle after the fault occurrence.

To better compare the performance of both FW and VW techniques on the single-ended impedance-based fault location method, the obtained errors are also shown in Fig. 7 as boxplots, as a function of the number of cycles used as input data. In such cases, the first two boxplots represent the estimated errors obtained from 1 cycle as input data of both FW and VW methods, respectively, the other two boxplots for 2 cycles using both FW and VW methods, respectively, and the last two boxplots for 3 cycles using both FW and VW methods, respectively.

From the obtained results depicted in Fig. 7, the higher errors were estimated for $d_{FW,1}$. However, for such period, the phasors estimated by the VW routine significantly improved the single-ended impedance-based fault locator performance. It is worth mentioning that the average error was below 5% for this analyzed period of time, which confirms that more accurate phasors can be estimated by techniques where data window lengths are able to be resized right after fault inceptions. These results could be even better if procedures to minimize the impacts of DC components (as mimic filters) combined with the VW function were used.

Therefore, the use of VW phasor-based solutions may appear as potential alternatives to be used in TLs equipped with high-speed protection functions, once the estimated fundamental components tend to converge faster than the ones obtained by FW routines. As a result, since faulty data samples at a shorter data window are available in the short-circuit period, more reliable and accurate fault distance estimations are obtained with VW phasor-based strategies.

IV. Additional Remarks

A. Impacts of decaying AC and DC components

To investigate in detail the performance of the evaluated single-ended impedance-based fault location function, considering both FW and VW phasor estimation methods, due to possible decaying AC and DC components of short-circuit currents, the power system described in section III was used. Basically, fault simulations were also carried out, but in the

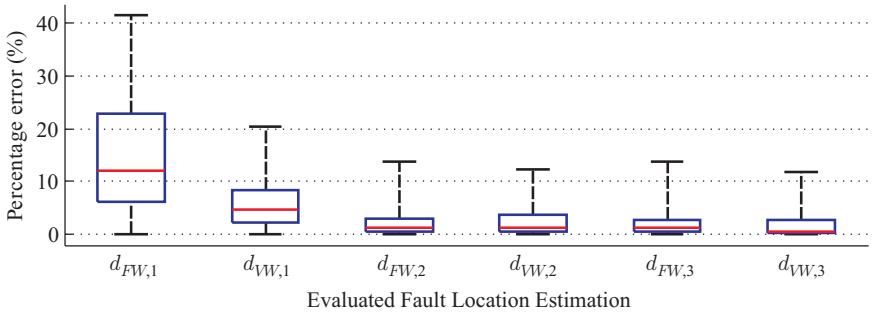

Fig. 7. Boxplots representing the obtained fault location errors as a function of the number of cycles used as input data.

parallel line near the generator, varying its location by values of 1 km, 5 km and 10 km away from the generator bus. Besides, the same faults simulations were carried out but the parallel lines were removed, i.e., considering just a single line connecting the buses. For each case, the Thevenin equivalent X/R ratio was also varied, in order to obtain different short-circuit characteristics.

From the obtained results, both FW and VW phasor estimation methods have presented similar performances when used as input data to the one-terminal impedance-based fault locator. Indeed, the decaying DC components tend to be eliminated by the mimic filter, as in the case of the analyzed FW algorithm. On the other hand, regarding the decaying AC components, their presence have not affected the analyzed phasor estimation methods (and consequently the fault location routine) in the evaluated short-circuit scenarios, even varying the Thevenin equivalent X/R ratio and the short-circuit distances from the generator bus. In all cases, the obtained errors were quite below 50 m, taking into account 2 and 3 cycles after the fault detection for both FW and VW techniques.

B. Impacts of CCVTs on the Evaluated Phasor-Based Methods

To investigate the impacts of CCVTs dynamic behaviors on the evaluated phasor estimation methods, fault simulations considering voltage measurements taken from the CCVT primary side and its secondary terminals were taken into account. For such analyses, a classical 230 kV CCVT reported in [20] for protection studies was implemented, whose topology and parameters are also reported in the same reference.

Basically, part of the short-circuit scenarios described in Table I were carried out. For illustration purposes, it is shown in Fig. 8 the voltages for an AG fault with inception angles of 90° and 0°, in which the corresponding phasors estimated by means of both FW and VW methods, considering the CCVT measurements, are named as $|\hat{V}_a|$ FW_{CCVT} and $|\hat{V}_a|$ VW_{CCVT}, respectively.

From the computed phasors shown in Figs. 8(a) and 8(b), the CCVT dynamic behavior introduces some oscillations in the phasor estimation techniques, especially in the first time instants after the disturbance occurrence, as classically reported in the literature [7], [21]. Such characteristic is also noticed in the VW technique. On the other hand, comparing the performances for the cases with and without CCVT, the difference between the obtained errors were below 1 km in

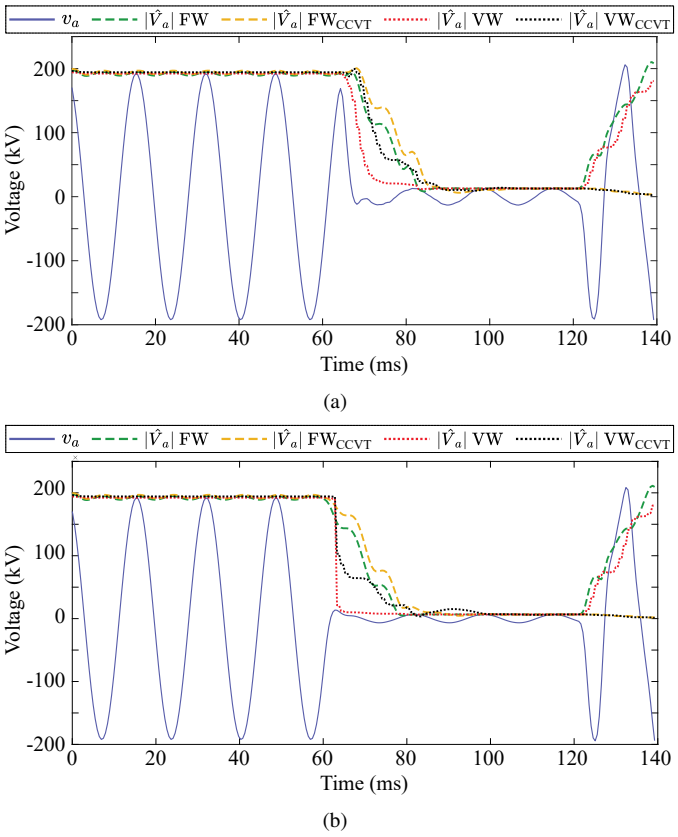

Fig. 8. Estimated phasors from FW and VW methods for an AG fault considering measurements from the CCVT with fault inception angles of: (a) 90°; (b) 0°.

the evaluated fault scenarios for 2 and 3 cycles after the fault inception. Obviously, such differences in the estimated results would be decreased if some of the methodologies to reconstruct CCVT secondary voltage signals would be used. However, it is noteworthy that the impact of the CCVT transient behavior affects the general phasor estimation methods, and not only the considered FW or VW routines.

V. Conclusions

In this paper, the performances of distinct FW and VW phasor-based techniques are thoroughly evaluated on a classical single-ended impedance-based fault location method, considering power networks equipped with high-speed protection

functions. To do so, several ATP short-circuit simulations were carried out in a 230 kV/60 Hz transmission system, varying their parameters such as location, type, inception angle and resistance.

From the obtained results, the fundamental frequency components estimated by both analyzed algorithms have provided similar performances for cases in which a bigger number of cycles are used as input data to the fault locator. In fact, for such scenarios, the data window used in the VW method reaches the same number of samples considered in the FW routine, resulting in similar estimated errors. On the other, for situations in which a smaller number of cycles are available in the fault period, due to the high-speed protection operation, for example, the VW method has provided the best estimations, since the window is resized (decreased) and contains only fault samples right after the disturbance occurrence. As a consequence, the transient period containing pre- and post-fault data samples is considerably reduced, minimizing possible oscillations in the computed phasors. These results could be even improved if procedures to minimize the impact of decaying DC components were used, whose strategies will be investigated by the authors in future works.

REFERENCES

[1] M. M. Saha, J. Izykowski, and E. Rosolowski, *Fault Location on Power Networks*, ser. Power Systems. London: Ed. Springer, 2010.

[2] S. Marx, B. K. Johnson, A. Guzmán, V. Skendzic, and M. V. Mynam, "Traveling wave fault location in protective relays: Design, testing, and results," in *16th Annual Georgia Tech Fault and Disturbance Analysis Conference*, May 2013.

[3] R. L. A. Reis, W. L. A. Neves, F. V. Lopes, and D. Fernandes Jr., "Sensitivity analysis of traveling wave-based and impedance-based fault location techniques," *International Conference on Power Systems Transients*, June 2019.

[4] X. Dong, S. Luo, S. Shi, B. Wang, S. Wang, L. Ren, and F. Xu, "Implementation and application of practical traveling-wave-based directional protection in UHV transmission lines," *IEEE Transactions on Power Delivery*, vol. 31, no. 1, pp. 294–302, Feb 2016.

[5] A. Phadke and J. Thorp, *Computer Relaying for Power Systems*, 2nd ed., ser. Protective relays. England: A John Wiley and Sons Ltd., 2009.

[6] D. G. Hart, D. Novosel, and R. A. Smith, "Modified cosine filters," Patent 6 154 687, November, 2000.

[7] R. L. A. Reis, W. L. A. Neves, and D. Fernandes Jr., "Influence of instrument transformers and anti-aliasing filters on the performance of fault locators," *Electric Power Systems Research*, vol. 162, pp. 142 – 149, 2018.

[8] M. Sachdev and M. Nagpal, "A recursive least error squares algorithm for power system relaying and measurement applications," *IEEE Transactions on Power Delivery*, vol. 6, no. 3, pp. 1008–1015, 1991.

[9] A. Funk and O. Malik, "Distance protection based on a variable window length filtering algorithm," *International Journal of Electrical Power and Energy Systems*, vol. 26, no. 9, pp. 669–679, 2004.

[10] B. Kasztenny, M. V. Mynam, T. Joshi, and C. Daniels, "A new digital filter using window resizing for protective relay applications," in *15th International Conference on Developments in Power System Protection (DPSP 2020)*, 2020, pp. 1–6.

[11] P. Jafarian and M. Sanaye-Pasand, "An adaptive phasor estimation technique based on LES method using forgetting factor," in *2009 IEEE Power and Energy Society General Meeting*, 2009, pp. 1–8.

[12] G. Benmouyal, "Removal of DC-offset in current waveforms using digital mimic filtering," *IEEE Transactions on Power Delivery*, vol. 10, no. 2, pp. 621–630, 1995.

[13] B. Kasztenny, "A new method for fast frequency measurement for protection applications," in *13th International Conference on Developments in Power System Protection*, 2016, pp. 1–8.

[14] K. M. Silva and B. F. Kusel, "Phasor estimation using a modified sine filter combined with an adaptive mimic filter," *International Conf. on Power Systems Transients*, June, 2011.

[15] T. Takagi, Y. Yamakoshi, M. Yamaura, R. Kondow, and T. Matsushima, "Development of a new type fault locator using the one-terminal voltage and current data," *IEEE Transactions on Power Apparatus and Systems*, vol. PAS-101, no. 8, pp. 2892 –2898, aug. 1982.

[16] A. Guzmán, B. Kasztenny, Y. Tong, and M. V. Mynam, "Accurate and economical traveling-wave fault locating without communications," in *2018 71st Annual Conference for Protective Relay Engineers (CPRE)*, March 2018, pp. 1–18.

[17] "IEEE guide for application of optical instrument transformers for protective relaying," *IEEE Std C37.241-2017*, pp. 1–50, 2018.

[18] E. O. Schweitzer III, B. Z. Kasztenny, and V. Skendzic, "High-fidelity voltage measurement using a capacitance-coupled voltage transformer," Patent 10 802 054, October, 2020.

[19] E. P. Machado, D. Fernandes, and W. L. A. Neves, "Tuning CCVT frequency response data for improvement of numerical distance protection," *IEEE Transactions on Power Delivery*, vol. 33, no. 3, pp. 1062–1070, June 2018.

[20] *EMTP Reference Models for Transmission Line Relay Testing*, IEEE Power System Relaying Committee, 2004. [Online]. Available: http://www.pes-psrc.org

[21] R. L. A. Reis, W. L. A. Neves, F. V. Lopes, and D. Fernandes Jr., "Coupling capacitor voltage transformers models and impacts on electric power systems: A review," *IEEE Transactions on Power Delivery*, vol. 34, no. 5, pp. 1874–1884, Oct 2019.